Collective dipole-dipole interactions in an atomic array

R. T. Sutherland[1,*] and F. Robicheaux[1,2,†]

[1]*Department of Physics and Astronomy, Purdue University, West Lafayette, Indiana 47907, USA*

[2]*Purdue Quantum Center, Purdue University, West Lafayette, Indiana 47907, USA*

(Received 29 April 2016; published 27 July 2016)

The coherent photon scattering of atoms in an atomic array is studied. It is found that due to cooperative photon exchanges, the excitation probability of an atom in an array parallel to the direction of laser propagation ($\hat{\boldsymbol{k}}$) will either grow or decay along $\hat{\boldsymbol{k}}$, depending on the detuning of the laser. The symmetry of the system for atomic separations of $a = j\lambda/2$ causes the excitation distribution and scattered radiation to abruptly become symmetric about the center of the array, where j is an integer and λ is the transition wavelength. For atomic separations of $a < \lambda/2$, a collection of *nonradiating* states ($\Gamma \sim 0$) disrupts the described trend. In order to interpret this surprising result, a band-structure calculation in the $N \to \infty$ limit is conducted, where the decay rates and the collective Lamb shifts of the eigenmodes versus quasimomentum are obtained. This calculation shows that the collective exchange of photons in an array strongly affects its scattered radiation, allowing one to easily manipulate the collective Lamb shift and directly excite either superradiant or subradiant eigenmodes by correctly choosing the angle of the driving laser.

DOI: 10.1103/PhysRevA.94.013847

I. INTRODUCTION

The coherent nature of the coupling between a collection of radiators and the electromagnetic field [1] has proven to be a fruitful field of study for over 60 years. Despite its history, the study of collective radiation is still providing important insights into quantum optics, leading to deeper understandings of waveguides [2], quantum information [3], biophysics [4,5], and cold atom clouds [6–14]. In particular, cold atom clouds have proven to be an important system for studying collective phenomena. For example, it has been noted that cooperative photon scattering can cause the excitation distribution of a cigar-shaped cloud to deviate from the results predicted by the Beer-Lambert law [6]. Further, the interplay between the collective Lamb shift [15–18], the energy shift due to the exchange of virtual photons between radiators [19], and its relationship to superradiance and subradiance [12,20–23] has produced a plethora of new physics. Notably, the study of the large-scale coherent buildup of *forward* photon emission in cold atom clouds has shown that coherent dipole-dipole interactions can produce superradiance in extended samples [6,7,24–26]. On the other hand, despite rapidly increasing interest, subradiance is still a difficult subject to study. Although recent work has made impressive progress [10,21,22], schemes for producing and studying subradiant states are rare.

Collective interactions in atomic arrays and/or lattices are also well studied and can produce exciting effects, such as the appearance of superradiant and subradiant eigenmodes [27–33]. However, these studies do not fully address the physics of position-dependent phase correlations in the array. When an extended system is illuminated by a laser, it excites the atoms to a state where the phase of the excitation amplitude of each atom is proportional to the laser's own phase (a timed-Dicke state) [26]. This produces coherences that dramatically change the photon scattering [16,22,24,34]. This effect has recently been studied by considering the emission of timed-Dicke states when an array has spacings, a, much less than the resonance wavelength (λ), where only nearest-neighbor interactions are considered [35]. However, the limit $a \ll \lambda$ is not relevant to most experimental setups. Also, in this regime the near field term in the dipole field propagator [see Eq. (2)] overshadows the interesting physics resulting from the coherent buildup of the $\propto 1/r$ term over the whole system. When $a \sim \lambda$ or larger, even though the individual dipole-dipole interactions are small, they can coherently build over an extended sample and cause surprisingly large effects. In this paper, we show that when both the phase correlations caused by the driving laser and the collective dipole-dipole interactions between *all* the atoms in an array are considered, they produce novel physics that allows for the manipulation of both the atoms' scattered light and excitation probability in a straightforward manner.

Specifically, it is shown that an array's probability distribution, when driven by a laser parallel to the array, is highly dependent on the detuning of the laser. For red (blue) detuned light, the dipole radiation in the direction of the laser causes the probability of excitation to increase (decrease) logarithmically (see Fig. 1). For atomic separations, a, of $j\lambda/2$, where j is an integer, the excitation distribution along the direction of the laser ($\hat{\boldsymbol{k}}$) rapidly changes so that it becomes completely symmetric about the center of the array.

In the interest of understanding the nature of the scattered emission of a finite array of atoms, the $N \to \infty$ limit is investigated through a band-structure calculation that gives both the collective Lamb shift and the decay rate of the eigenmodes for a given quasimomentum. It is then shown that the appearance and disappearance of Bragg diffraction peaks causes the eigenmodes to discontinuously jump from subradiant (superradiant) to superradiant (subradiant) when plotted versus quasimomentum. For extended samples (much larger than λ), it is straightforward to produce subradiant states with decay rates much less than a single atom. Where in the Dicke limit (samples much smaller than λ) subradiant states are the set of antisymmetrical states, subradiant states

*rsutherl@purdue.edu

†robichf@purdue.edu

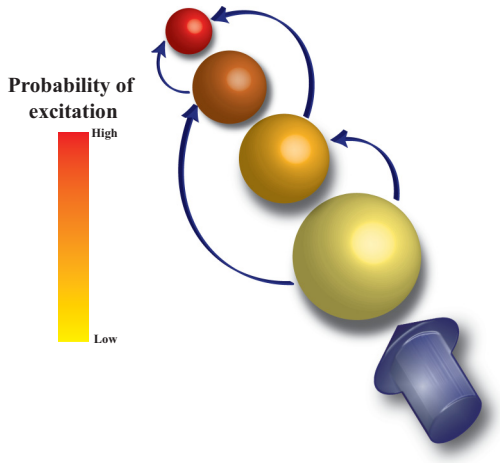

FIG. 1. When a red detuned laser drives an array of atoms, the probability of excitation grows logarithmically down the line of the array. This effect and the others discussed in this paper, are due to the spatially dependent phase correlations between the driving laser and the dipole radiation.

for our extended periodic system are those with a specific quasimomentum (see Sec. V). Lastly, it is demonstrated how the relationship between an eigenmode's quasimomentum and its decay rate allows one to directly and specifically excite subradiant eigenmodes by correctly choosing the angle of the driving laser.

II. THEORY AND METHODS

For a weak laser, a collection of two-level atoms polarized in the $\hat{\boldsymbol{x}}$ direction can be treated as coupled damped harmonic oscillators [9,34,36,37],

$$\dot{b}_n(t) = (i\Delta - \Gamma/2)b_n(t) - i(d/\hbar)E(\boldsymbol{r}_n) - (\Gamma/2)\sum_{m\neq n} G(\boldsymbol{r}_m - \boldsymbol{r}_n)b_m(t), \tag{1}$$

where b_n represents the polarization amplitude of atom n, d is the electric dipole matrix element, $E(\boldsymbol{r}_n) = E_0 e^{i\boldsymbol{k}\cdot\boldsymbol{r}_n}$ is the the laser field at atom n, Δ is the detuning, Γ is the single-atom decay rate, and $G(\boldsymbol{r})$ is the usual dipole field propagator [38]:

$$G(\boldsymbol{r}) = \frac{3e^{ikr}}{2ikr}\left\{[1-(\hat{\boldsymbol{r}}\cdot\hat{\boldsymbol{x}})^2] + [1-3(\hat{\boldsymbol{r}}\cdot\hat{\boldsymbol{x}})^2]\left[\frac{i}{kr} - \frac{1}{(kr)^2}\right]\right\}, \tag{2}$$

where $r = |\boldsymbol{r}|$, and $\hat{\boldsymbol{r}}$ is the vector $\hat{\boldsymbol{r}} = \boldsymbol{r}/r$. These coupled equations can be rewritten in matrix-vector form,

$$\dot{\boldsymbol{b}} = \underline{\boldsymbol{M}}\boldsymbol{b} - i\frac{d}{\hbar}\boldsymbol{E}, \tag{3}$$

and the steady-state solution ($\dot{\boldsymbol{b}} = 0$) may be obtained by inverting a complex symmetric $N \times N$ matrix.

One may gain insight into this system by examining the eigenvalues and eigenvectors defined by

$$\underline{\boldsymbol{M}}\boldsymbol{v}_\mu = \left\{i(\delta_\mu + \Delta) - \frac{\Gamma_\mu}{2}\right\}\boldsymbol{v}_\mu. \tag{4}$$

Here $\boldsymbol{v}_\mu$ represents the μth eigenmode, $(\delta_\mu + \Delta)$ corresponds to the imaginary part of the eigenvalue and gives the laser's detuning from the collective Lamb shift of the eigenmode, and Γ_μ corresponds to the real part of the eigenvalue and gives the decay rate. Since $\underline{\boldsymbol{M}}$ is complex symmetric rather than Hermitian, $\boldsymbol{v}_\nu^\dagger\boldsymbol{v}_\mu = \delta_{\nu\mu}$ does not hold under the assumption of nondegenerate eigenvalues. However, $\boldsymbol{v}_\nu^T\boldsymbol{v}_\mu = \delta_{\nu\mu}$ does [39]. Using this identity, we may rewrite Eq. (3) as

$$\dot{c}_\mu(t) = \left\{i(\delta_\mu + \Delta) - \frac{\Gamma_\mu}{2}\right\}c_\mu(t) - i\alpha_\mu(t), \tag{5}$$

where $c_\mu = \boldsymbol{v}_\mu^T\boldsymbol{b}$ and $\alpha_\mu = \frac{d}{\hbar}\boldsymbol{v}_\mu^T\boldsymbol{E}$. This may be rewritten in the $t \to \infty$ limit as

$$c_\mu(\infty) = \frac{\alpha_\mu}{(\delta_\mu + \Delta) + i\Gamma_\mu/2}. \tag{6}$$

The steady-state population of the eigenmode, $c_\mu(\infty)$, will be at a maximum when $\Delta = -\delta_\mu$ and will have a linewidth of $\Gamma_\mu/2$. This shows that the amplitude of an eigenmode is dependent on both its projection onto the driving laser, α_μ, as well as its detuning with respect to Δ.

For the band-structure calculations of Sec. V, the $N \to \infty$ limit is implemented in order to calculate the eigenvalues of $\underline{\boldsymbol{M}}$ for a specific quasimomentum, q. In this limit, the translational symmetry of the system may be used in order to rewrite the eigenvalue problem

$$\sum_n M_{mn}v_{nq} = \left\{i(\delta_q + \Delta) - \frac{\Gamma_q}{2}\right\}v_{mq} \tag{7}$$

as

$$\sum_n M_{mn}e^{inaq}v_0 = \left\{i(\delta_q + \Delta) - \frac{\Gamma_q}{2}\right\}e^{imaq}v_0,$$
$$\sum_n M_{mn}e^{i(n-m)aq} = \left\{i(\delta_q + \Delta) - \frac{\Gamma_q}{2}\right\}, \tag{8}$$

where we have replaced v_{nq} with v_0e^{inaq}. The calculation has now been reduced to an infinite sum that converges for most values of q (see Sec. V).

III. EXCITATION DISTRIBUTION

A. Numerical results

An understanding of the highly directional nature of the interactions that add coherently can be gained by noting the similarities in the phases accumulated between the driving laser and the dipole-dipole interactions [6]. Essentially, the phase a laser will accumulate when going from atom n to atom m is $e^{i\boldsymbol{k}\cdot(\boldsymbol{r}_n - \boldsymbol{r}_m)}$, while the phase accumulated in a photon exchanged by the two atoms is $e^{ik|\boldsymbol{r}_n - \boldsymbol{r}_m|}$. These two phases are equivalent when $(\boldsymbol{r}_n - \boldsymbol{r}_m)$ is parallel to $\hat{\boldsymbol{k}}$. Because of this, all of the radiation and virtual photon exchanges along $\hat{\boldsymbol{k}}$ add coherently, while they add incoherently along $-\hat{\boldsymbol{k}}$ relative to atom n. Therefore, the excitation probability of atom n,

$$P(n) \equiv |b_n|^2, \tag{9}$$

depends mainly on the dipole-dipole interactions from the $n-1$ atoms in the $-\hat{\boldsymbol{k}}$ direction relative to n. This is shown in Fig. 2(a), where except for small oscillations caused by

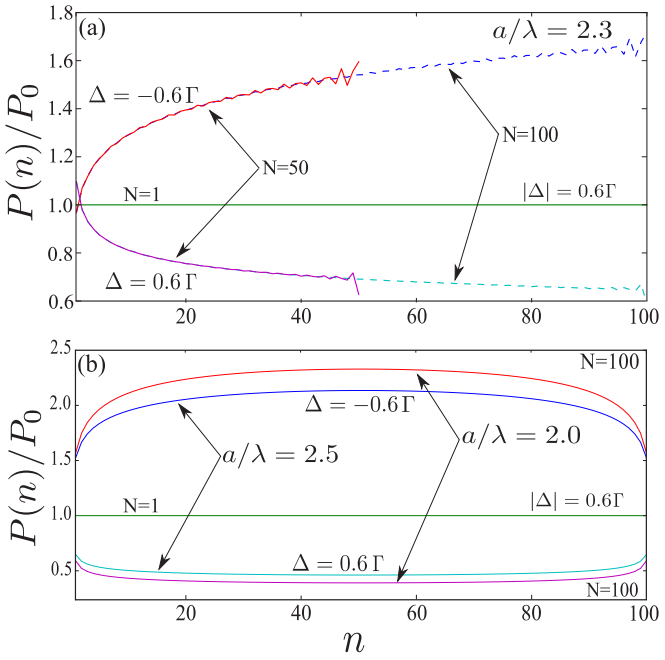

FIG. 2. (a) Probability of excitation of atom n [$P(n)$] divided by the single-atom excitation probability (P_0) for that detuning (Δ). For the top two plots, $P(n)/P_0$ is shown for a detuning of -0.6Γ using 50 and 100 atoms. Note that except for small oscillations, both plots lie on top of each other for up to $n = 50$. This is due to the highly forward character of the coherent interactions. For the bottom two plots, $P(N)/P_0$ is shown for a detuning of $+0.6\Gamma$ using 50 and 100 atoms. The noninteracting probability for the same Rabi frequency and $|\Delta|$ is shown for reference. (b) The symmetric probability distribution present for integer and half-integer values of a is shown for red and blue detunings.

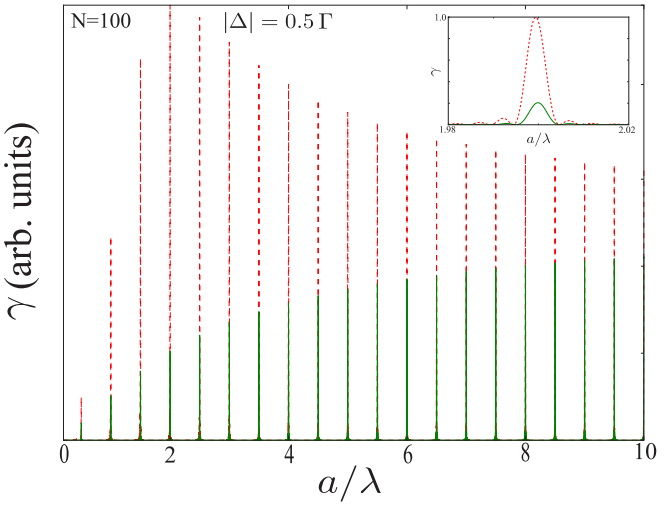

FIG. 3. Photon scattering rate (γ) in the $-\hat{\boldsymbol{k}}$ direction versus array spacing a for an array of 100 atoms for values of detuning $\Delta = 0.5\Gamma$ (green solid line) and $\Delta = -0.5\Gamma$ (red dotted line). The inset shows the same graph zoomed in around $a = 2\lambda$. Note that the difference in the heights of the peaks is mainly due to the fact that the collective Lamb shift of the driven eigenmode changes with a.

reflections off of the end of the array, the value of $P(n)$ follows approximately the same curve for an array of 50 atoms as an array of 100 atoms for both red and blue detunings. Note that this mechanism is only true when $a \neq j\lambda/2$, where j is an integer, as will be discussed shortly.

The nature of $P(n)$ can be intuitively understood by considering that the nth atom in the array will only see a significant contribution of electric field from the driving laser and the $n-1$ atoms located in the $-\hat{\boldsymbol{k}}$ direction relative to it, as well as the fact that the dominant term in the dipole-dipole interaction is $\propto 1/(kr)$ for large spacings. It can now be seen that atom n will feel a sum of dipole-dipole interactions that add either constructively or destructively with the driving laser. This results in the polarization amplitude having the form

$$b_n - b_1 \propto \frac{1}{ka}\sum_{m<n}\frac{1}{m}, \tag{10}$$

which is $\sim \ln(n)$ for large values of n. This gives the approximate form of $P(n)$ shown in Fig. 2(a). Also note that in Fig. 2, the magnitude of the the change in $P(n)$ for a given array is larger for red detunings than blue detunings of the same magnitude, since the resonance frequency for an array of atoms parallel to $\hat{\boldsymbol{k}}$ is redshifted (see Sec. V).

The above description holds only for values of $a \neq \frac{j\lambda}{2}$, where j is an integer. This can be understood from the fact that the only terms in Eq. (1) distinguishing b_1 from b_N, b_2 from b_{N-1}, etc. are the phase factors e^{ikna}, where n is the atom label. If $e^{ikna} \to \pm 1$ for all n, Eq. (1) is symmetric about the center of the array. Resultantly, when $a \to \frac{j\lambda}{2}$, $P(n)$ must have mirror symmetry. Because of this, the only parameter determining the value of $P(n)$ is the total magnitude of all the dipole-dipole interactions atom n experiences. For red detunings this causes the atoms experiencing the strongest interactions (atoms in the center of the array) to be the most excited. For blue detunings, dipole-dipole interactions add such that the atoms in the center are the least excited. Both of these effects may be seen in Fig. 2. Because both the forward and backward dipole-dipole interactions now add coherently, the dependence described in Eq. (10) becomes

$$b_n - b_1 \propto \frac{1}{ka}\sum_{m\neq n}\frac{1}{|m-n|}. \tag{11}$$

The symmetry about the center of the array also causes a large increase in the coherent backscattering (see Fig. 3). Normally the phase correlations of an array of atoms parallel to $\hat{\boldsymbol{k}}$ only allow for coherent forward scattering [16,25]; however, because of the symmetry about $\pm\hat{\boldsymbol{k}}$ when $a \to \frac{j\lambda}{2}$, light scattered in the $-\hat{\boldsymbol{k}}$ direction also adds coherently, causing a Bragg diffraction peak. The inset in Fig. 3 shows a closeup of one of the peaks. Near a given peak, the coherent backscattering has the approximate form $\{j_0(kN\alpha)\}^2$, where $\alpha = a - j\lambda/2$ and $j_0(x)$ is the zeroth spherical Bessel function. This can be shown using the equation for the angular distribution of the photon scattering rate:

$$\frac{d\gamma}{d\Omega} = \frac{3\Gamma}{8\pi}\{1-(\hat{\boldsymbol{k}}\cdot\hat{\boldsymbol{x}})^2\}\sum_{n,m} e^{i\vec{\boldsymbol{k}}\cdot(\vec{r}_m-\vec{r}_n)} b_n b_m^*, \tag{12}$$

where γ is the photon scattering rate, and making the approximation that the atoms are in the timed-Dicke state

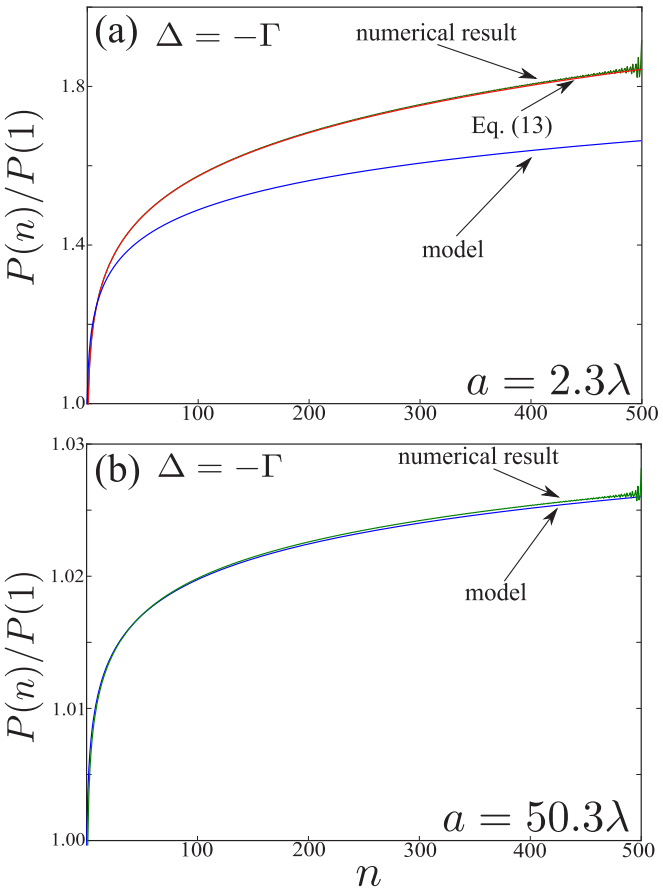

FIG. 4. The probability of excitation of atom n [$P(n)$] divided by the probability of excitation of the first atom [$P(1)$] for an array containing 500 atoms. (a) Comparison between the full numerical calculation (green), Eq. (13) (red), and our analytic model (blue) for $a = 2.3\lambda$. Since the approximations made in the analytic derivation hold only for $ka \gg 1$, the analytic model is only qualitatively accurate in this regime. Note that when $P(n)$ is generated from Eq. (13), it lies on top of the full calculation (excluding small oscillations at large n) for all $a > \lambda$. (b) Comparison between the full numerical calculation (green) and the analytic model (blue) for $ka \gg 1$. This illustrates the fact that the analytic model approaches the quantitative numerical result for this condition, as well as the fact that the logarithmic growth holds for very large array spacings. Note that these results are only true for $a \neq \frac{j\lambda}{2}$.

($b_n = |b_0|e^{ikna}$) caused by a laser propagating in the $+\hat{\boldsymbol{k}}$ direction. The differences in the heights of the diffraction peaks shown in Fig. 3 are mainly caused by the fact that the collective Lamb shift of the eigenmode that the laser drives changes with a. In Fig. 3, the intensity of successive diffraction peaks increases until $a = 2\lambda$, where it then begins to decrease. For different laser detunings, this pattern follows a different form.

Figure 2(a) is for $a = 2.3\lambda$ and detunings of $|\Delta| = 0.6$, which for red detunings show an ∼70% difference between the first and last atoms. However, due to the long-range nature of the coherent buildup of dipole radiation, the logarithmic growth of $P(n)$ does not saturate for large values of a. For example, in Fig. 4(b), an ∼2.6% growth in $P(n)$ is seen for $a = 50.3\lambda$. In fact, until other time scales, such as retardation effects, become important, there is no value of a where this logarithmic growth does not, in principle, happen.

The nature of $P(n)$ described here is qualitatively valid in nonideal circumstances. This is tested using Monte Carlo routines where the filling factor and the randomness of the position of each atom is varied. The magnitude of the overall growth for noninteger wavelengths is approximately proportional to the filling factor of the sample. For example, if an experiment would have produced an array where the first and last atoms have an excitation probability that differs by 50%, a filling factor of 0.5 causes the overall effect to reduce to ∼25%. It is also found that for $a \neq \frac{j\lambda}{2}$, when each atom's x,y,z values are allowed to randomly vary, the noise of a given array's $P(n)$ increases while the average value of $P(n)$ does not change until the randomness of the atoms' positions is allowed to vary distances comparable to a, not λ. For example, if $a = 20.3$, the sample is significantly more resilient to random positions than if $a = 2.3$. However, it is found that the described symmetry for $a = \frac{j\lambda}{2}$ is more sensitive to nonideal scenarios. Unlike the logarithmic buildup, the robustness of the symmetry about the center of the array does not seem to depend on the value of a. It is found that for all spacings, letting the atom positions randomly vary more than ∼0.3λ causes the symmetric $P(n)$ distribution to begin to approach the logarithmic function seen for $a \neq \frac{j\lambda}{2}$. Note that the probability distributions described here occur only when $\hat{\boldsymbol{k}}$ is parallel to the array.

B. Analytic derivation of excitation distribution

In this section, the approximation that dipole-dipole interactions adding incoherently (occurring in the $-\hat{\boldsymbol{k}}$ direction) are negligible is implemented in order to derive an equation for $P(n)$ analytically. Note that this is only valid when $a \neq \frac{j\lambda}{2}$. Neglecting all incoherent interactions allows us to replace $\underline{\boldsymbol{M}}$ in Eq. (3) with a lower triangular matrix. When the $\boldsymbol{b} \to 0$ limit is taken, solving for $\boldsymbol{b}$ is reduced to solving the system of equations

$$
\begin{aligned}
0 &\simeq \left(i\Delta - \frac{\Gamma}{2}\right)b_1 - i(d/\hbar)E(\boldsymbol{r}_1),\\
0 &\simeq \left(i\Delta - \frac{\Gamma}{2}\right)b_2 - i(d/\hbar)E(\boldsymbol{r}_2) - \frac{\Gamma}{2}G(a)b_1,\\
0 &\simeq \left(i\Delta - \frac{\Gamma}{2}\right)b_3 - i(d/\hbar)E(\boldsymbol{r}_3) - \frac{\Gamma}{2}G(a)b_2 - \frac{\Gamma}{2}G(2a)b_1,\\
&\ldots ,
\end{aligned}
\tag{13}
$$

where b_n is the amplitude of the nth atom. This can be solved for b_1, which can be plugged into the equation for b_2 etc. The approximation indicated in Eq. (13) remains quantitatively accurate when $a > \lambda$. This can be seen in Fig. 4(a) where, except for small oscillations due to reflections off the end of the array, the curve produced by solving Eq. (13) remains nearly identical to the full numerical result. Assuming Eq. (13) and keeping only the first-order terms in $1/(ka)$ allows one to

obtain a closed-form solution for b_n:

$$b_n e^{-ik(n-1)a} \simeq \frac{i d E_0/\hbar}{i\Delta - \Gamma/2}\left(1 - \frac{3i\Gamma}{4ka(i\Delta - \Gamma/2)}\sum_{m=1}^{n-1}\frac{1}{m}\right). \tag{14}$$

To the same order in $(1/ka)$, one can now obtain a solution for $P(n)$:

$$P(n) \simeq \frac{(d E_0/\hbar)^2}{\Delta^2 + \Gamma^2/4}\left(1 - 2\mathrm{Re}\left\{\frac{3i\Gamma}{4ka(i\Delta - \Gamma/2)}\sum_{m=1}^{n-1}\frac{1}{m}\right\}\right). \tag{15}$$

These equations hold in the limit $ka \gg 1$ and describe how $P(n)$ grows for red detunings and diminishes for blue detunings. This can be seen by rewriting the second term in Eq. (15) in terms of its real and imaginary parts. The real part of the second term, which is the dominant contributor to $P(n)$, adds to the probability amplitude for red detunings and subtracts from the probability amplitude for blue detunings. Physically, this means that in the steady-state limit the singly scattered photons add *in phase* with red detuned lasers and *out of phase* with blue detuned lasers. As seen in Fig. 4, for smaller spacings the simple model used to derive Eq. (14) becomes only qualitative. This is because in this regime, higher-order $1/(ka)$ terms matter. As a becomes smaller than λ, individual dipole-dipole interactions grow, and despite the fact that they add incoherently, the contributions of a couple of large interactions in the $-\hat{\boldsymbol{k}}$ direction begin to become significant, causing Eq. (13) to break down.

IV. $a < \lambda/2$ BEHAVIOR

As can be seen in Fig. 5, the excitation distribution described above breaks down for values of $a < \lambda/2$. This may be understood by considering the distribution of eigenvalues, $i(\delta_\mu + \Delta) - \Gamma_\mu/2$, of $\underline{\boldsymbol{M}}$. Here, Γ_μ is the μth eigenmode's decay rate, while $(\delta_\mu + \Delta)$ gives the laser's detuning from the collective Lamb shift of the eigenmode. When $a < \lambda/2$, there exists a collection of nonradiating ($\Gamma_\mu \sim 0$) eigenmodes of $\underline{\boldsymbol{M}}$ within a relatively small energy range (see Fig. 6). This effect has been studied in systems such as arrays of metallic nanospheres [40–42], where it has been shown that these eigenmodes may be used for their optical transport properties. The same physics strongly affects the excitation distribution of an array driven by a laser. In Fig. 5, the excitation distribution for an array of 100 atoms, where $a = 0.4\lambda$, is shown for various values of Δ. In Fig. 5(a), it may be seen that the values of Δ that lie within the energy range of the collection of subradiant states ($\Delta = -0.4\Gamma - 0.9\Gamma$) produce very different excitation distributions than the logarithmic ones described in the previous sections. However, Fig. 5(b) shows that once the laser is off resonance with the collection of subradiant states, the distribution becomes logarithmic again.

Figure 6 shows the decay rates (Γ_μ) and collective Lamb shifts (δ_μ) for the eigenmodes of an array where $a = 0.4\lambda$, $\Delta = 0$, and $N = 100$. Here it can be seen that despite the fact that the overall size of the system is 40λ, there is a collection of eigenmodes such that $\Gamma_\mu \sim 0$ within a very narrow range of energies. Even though populating an individual subradiant state can be difficult due to the narrowness in energy of its

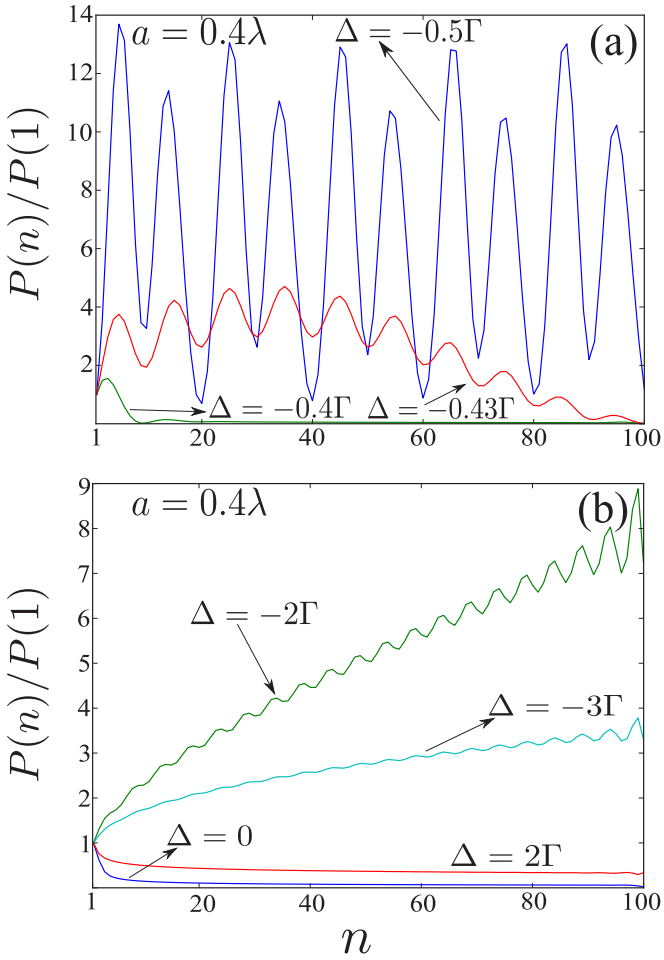

FIG. 5. The probability of excitation of atom n [$P(n)$] divided by the probability of excitation of atom 1 [$P(1)$]. (a) Excitation distribution for a laser resonant with the collection of subradiant states ($\Gamma_\mu \sim 0$) for an array of 100 atoms separated by a distance of 0.4λ. Over the range of laser detunings $\Delta = -0.4\Gamma - 0.9\Gamma$, the behavior is drastically altered due to the almost complete lack of decay by photon emission. (b) The same array of atoms for laser detunings that do not lie within ($\Delta \sim -0.4\Gamma - 0.9\Gamma$) show qualitatively similar results to those described previously.

photon scattering cross section, the fact that they all occur in a very small energy range causes them to be the dominant feature of the steady-state solution for values of Δ within their energy band. The presence of $\Gamma_\mu \sim 0$ decay modes will be explained in Sec. V.

V. BAND STRUCTURE

In order to understand the eigenmodes and eigenvalues of this system, we examine its band structure [see Eq. (8)] in the $N \to \infty$ limit. Since in Eq. (1) there is only one oscillator per atom, there is only one band of eigenvalues. Setting $\Delta = 0$, for a given eigenvalue $(i\delta_q - \Gamma_q/2)$, the real part (Γ_q) corresponds to the decay rate of eigenmode q, while the imaginary part $(i\delta_q)$ corresponds to its collective Lamb shift. Here the q represents the quasimomentum of the eigenmode, giving the change in the phase of the probability amplitude going from atom to

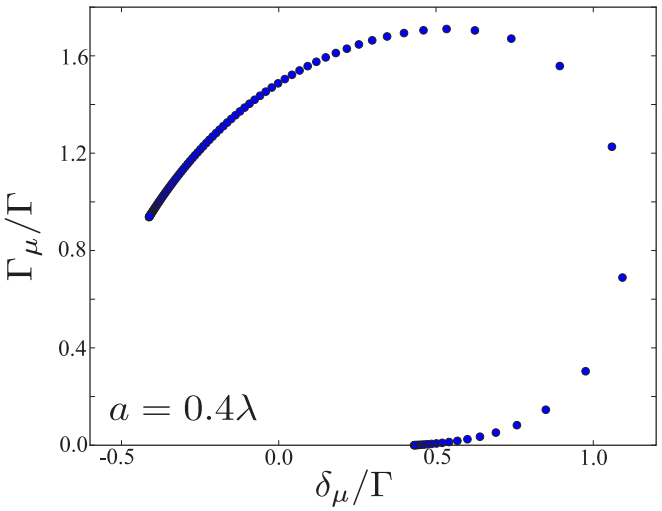

FIG. 6. The decay rate (Γ_μ) and the collective Lamb shift (δ_μ) of the eigenmodes of an array divided by the single-atom decay rate (Γ), where $a = 0.4\lambda$, $\Delta = 0$, and $N = 100$. Note the collection of eigenvalues near the $\Gamma_\mu = 0$ axis, despite the fact that the length of the array is 40λ.

atom. Note that values of δ_q that are positive correspond to redshifts in the resonance line of that eigenmode.

In Fig. 7, the values of Γ_q and δ_q are plotted for the positive half of the Brillouin zone ($0 \geqslant q < \pi/a$). Note that q is the quasimomentum of eigenmode $\boldsymbol{v}_q$ shown in Eq. (8). The negative values of q may be omitted since the calculation is symmetric and yields the same results. As will be discussed in Sec. VI, the value of q for an array may be changed by adjusting the direction of laser propagation with respect to the array. In Fig. 7(a), a discontinuity is seen at $ka = qa$, when the value of Γ_q drops to 0, changing the eigenmode from superradiant to nonradiant. At the same time in Fig. 7(b), when $ka + (qa) = 2\pi$ the value of Γ_q shows a discontinuity from a subradiant mode to a superradiant mode. The same pattern occurs for larger array spacings. In Fig. 7(c), when $(ka) - 2\pi = qa$ the eigenmodes shift from superradiant to subradiant, while in Fig. 7(d), when $ka + (qa) = 4\pi$ the eigenmodes jump from subradiant to superradiant. While the magnitude of each discontinuous jump of Γ_q decreases with a, approaching $\Gamma_q = \Gamma$ when $a \to \infty$, the described band-structure pattern repeats for every integer increase in a/λ. This can be understood in terms of the appearance and disappearance of Bragg diffraction peaks. This phenomena was somewhat addressed in [27], but the effect of different phase correlations (values of q) on the decay rate was not.

Figure 7 can be understood by examining Eq. (12), which gives the photon emission rate per unit solid angle for a line of two-level atoms polarized in the $\hat{\boldsymbol{x}}$ direction:

$$\frac{d\gamma}{d\Omega} = \frac{3\Gamma}{8\pi}\{1 - \sin^2\theta\cos^2\phi\}|b_0|^2 \sum_{n,m} e^{i(m-n)a(k\cos\theta - q)}, \quad (16)$$

where b_0 is a magnitude determined by the detuning and the Rabi frequency, while q is the quasimomentum of the eigenmode. All of the phases in Eq. (16) will add coherently, resulting in a Bragg diffraction peak when

$$a(k\cos\theta - q) = 0, \pm 2\pi, \pm 4\pi, ..., \quad (17)$$

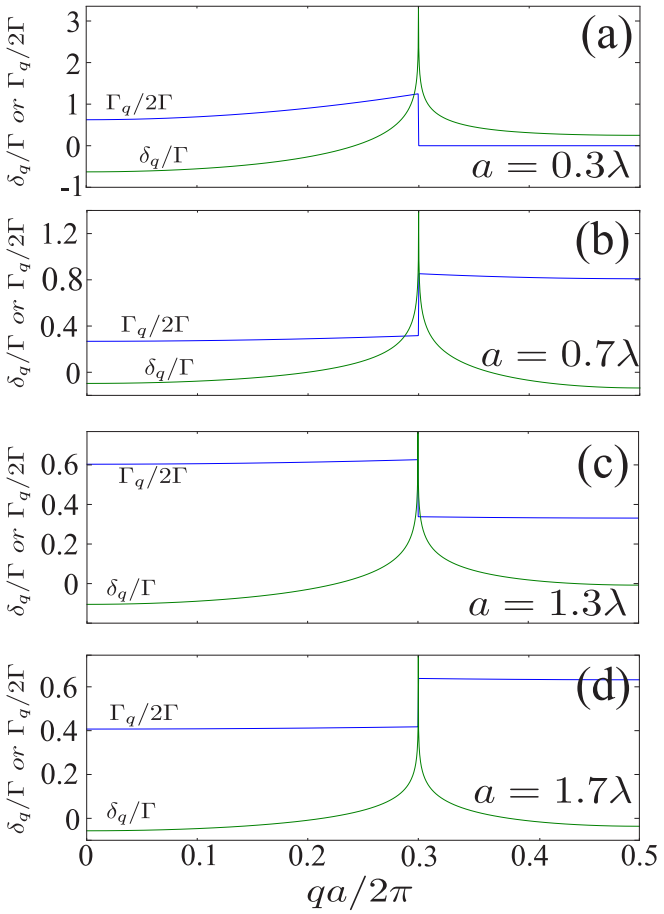

FIG. 7. The values of Γ_q and of δ_q (the collective Lamb shift) are plotted versus values of $0 \leqslant qa/2\pi < 0.5$. (a) Shows this for array spacings of $a = 0.3\lambda$, (b) $a = 0.7\lambda$, (c) $a = 1.3\lambda$, and (d) $a = 1.7\lambda$. Note that for all four graphs the collective Lamb shift diverges at $qa/2\pi = 0.3$, while Γ_q gives a discontinuous jump caused by the appearance or disappearance of a Bragg diffraction peak.

which means there will be a peak at the angle

$$\theta = \arccos\left\{\lambda\left(\frac{m}{a} + \frac{q}{2\pi}\right)\right\}; m = 0, \pm 1, \pm 2... \quad (18)$$

If every atom has the same phase ($q = 0$), then for values of $n\lambda < a < (n+1)\lambda$ there will be $2n+1$ values of θ where Eq. (18) can be satisfied and photons may be scattered. Thus when $q = 0$, the photon scattering of the array produces the well-known behavior of a diffraction grating. However, this is not the case when $q \neq 0$. For example, when $0 < a < \lambda/2$ and $qa > ka$, there are no solutions to Eq. (18). The result of this is that for infinite arrays, states with values of $qa > ka$ and $a < \lambda/2$ *do not decay*. This is seen in Fig. 7(a), when Γ_q jumps discontinuously to 0. The opposite effect happens when $\lambda/2 < a < \lambda$. Here for small values of q, there is only one angle where the array can emit radiation coherently. However, when the value of q is increased to the point where $a(k + |q|) > 2\pi$ there is suddenly another value of θ corresponding to a diffraction peak, resulting in a discontinuous increase in the value of Γ_q (see Fig. 7). This pattern continues for larger values of a as well. If $a = m\lambda + \eta$ ($m = 0, 1, 2...$), where $\eta < \lambda/2$, then when q is increased to the point where $qa > k\eta$ there

is one less diffraction peak where photons may escape. This makes the eigenmode's decay rate smaller. However, if $\lambda/2 < \eta < \lambda$, when $|qa| + k\eta > 2\pi$ there is one more allowed peak, making the decay rate of the eigenmode larger. For spatially disordered systems such as cold atom gases, this discontinuity does not occur. However, when the atoms in a gas are excited to a timed-Dicke state, a similar peak still occurs in the forward direction [26], which also results in an increase in the decay rate [6,16,20].

Another surprising feature of Fig. 7 is the divergence of the collective Lamb shift at the same values of q where the discontinuities of Γ_q occur. This happens because the phase in the sum given by Eq. (8) becomes a multiple of 2π at this point, making the value of the imaginary part of ϵ_q dependent on a logarithmically diverging infinite sum over $\frac{1}{na}$. The decay rate does not diverge, however. This is because when the phase in Eq. (8) becomes a multiple of 2π the real part of the $\propto 1/r$ term disappears, leaving only the convergent $1/r^2$ sum for the value of the decay rate.

VI. CONTROLLING THE COLLECTIVE LAMB SHIFT AND PROBING SUBRADIANT EIGENMODES

The band structure of an array has a strong effect on the scattered radiation versus the angle of the driving laser. This is because if one changes the angle of the laser, to first order they are also changing the quasimomentum of the eigenmode being driven. For an array aligned along $\hat{z}$, the phase of the laser at the nth atom is $ikna\cos\theta$. As a result, when θ is changed, the laser's projection onto the qth eigenmode [α_q from Eq. (5)] is also changed. For example, if the laser is perpendicular to the atomic array, the eigenmode corresponding to $qa = 0$ is being driven. If the laser is situated at some arbitrary angle θ, the value of qa of the eigenmode being driven is equal to $ka\cos\theta$. Figure 8(a) shows how the photon scattering rate changes with respect to θ. Here large changes in the scattering rate occur when the laser changes from driving a subradiant (superradiant) quasimomentum to a superradiant (subradiant) quasimomentum. Figure 8(a) also shows that the scattering rate dramatically drops at the point where this change happens due to the large collective Lamb shift for this value of qa. It should be noted that increases in qa of 2π correspond to the same phase correlations. For example, Fig. 8(b) shows that for an array with spacings $a = 1.3\lambda$, $\theta = 0$ and $\theta = \arccos(1.0/1.3)$ give the exact same line shape.

For values of $a > \lambda/2$, the photon scattering line shapes versus laser detuning fit a Lorentzian profile almost perfectly, with decay rates and collective Lamb shifts corresponding to their band-structure values. As seen in Fig. 8(b) for an array of 1000 atoms and $a = 1.3\lambda$, when $\theta = 0$ or $\theta = \arccos(0.3/1.3)$, $\Gamma_q \simeq 0.94\Gamma$ and $\delta_q \simeq -0.54\Gamma$. The large shift in resonant energy occurs because of the logarithmically diverging collective Lamb shift discussed above, while $\Gamma_q \simeq 0.94\Gamma$ because the value of qa occurring at the discontinuous jump between subradiant and superradiant modes is driven, which produces a decay rate equal to the average of the two. When $\theta = \pi/2$ or $\theta = \arccos(1.0/1.3)$, the superradiant band is driven, resulting in a broadened line shape with $\Gamma_q \simeq 1.2$ and $\delta_q \simeq 0.1\Gamma$, while when $\theta = \arccos(0.5/1.3)$ the subradiant band is driven, giving $\Gamma_q \simeq 0.66\Gamma$ and $\delta_q = 0.01\Gamma$. This indicates several interesting points. First, that it is possible to create subradiant eigenmodes with decay rates *smaller* than the single-atom decay rate, even when the atoms are separated by distances larger than λ. Second, unlike in the Dicke limit where the decay rate of an eigenmode is determined by its symmetry, for extended and periodic systems whether a given eigenmode is subradiant or superradiant depends on its quasimomentum. Lastly, this shows how one may easily access either subradiant or superradiant eigenmodes by correctly choosing the angle of the driving laser.

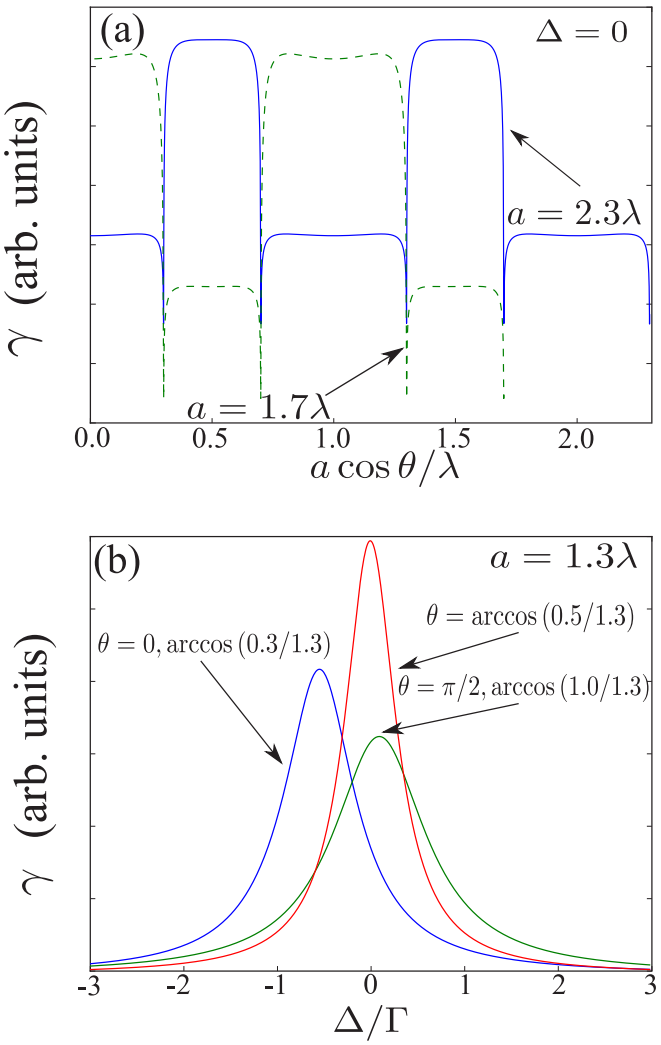

FIG. 8. The dependance of the scattered photon emission on the laser angle θ, which is the angle between an array of 1000 atoms and the driving laser. (a) The scattered radiation versus $a\cos\theta/\lambda$ for a laser with $\Delta = 0$ and arrays with spacings of 1.7λ and 2.3λ. Note that the large shifts in scattered radiation occur when the eigenmode that the laser drives crosses a band-structure discontinuity. (b) The photon scattering rate versus detuning of an array where $a = 1.3\lambda$ for three different laser angles (θ): $\{0, \arccos(0.3/1.3)\}$, $\{\pi/2, 1.0/1.3\}$, and $\arccos(0.5/1.3)$. The scattering rates for all three angles fit to a Lorentzian line shape well, with decay rates and line shifts that correspond to those given by their $N \to \infty$ limit band-structure calculations seen in Fig. 7.

VII. CONCLUSION

The effects in a coherently radiating atomic array being driven by a laser have been studied. It was shown numerically that the excitation distribution for a given array is highly dependent on whether the driving laser is red or blue detuned. It was then shown analytically that the probability of excitation grows along $\hat{\boldsymbol{k}}$ for red detunings and diminishes along $\hat{\boldsymbol{k}}$ for blue detunings even for extremely large values of a. This is because the singly scattered photons along $\hat{\boldsymbol{k}}$ add in phase with red detuned lasers and out of phase with blue detuned lasers. It was also shown that the probability distribution and photon scattering become symmetric about the center of the array for spacings of $j\lambda/2$. These results break down when $a < \lambda/2$ due to the presence of a collection of extremely subradiant states ($\Gamma_q \sim 0$).

In order to interpret the eigenmodes of the system, a band-structure calculation for an infinitely long array of atoms was conducted. These calculations showed the eigenmodes have both a collective Lamb shift that diverges logarithmically, as well as a discontinuous decay rate when plotted versus quasimomentum. The sudden jump from subradiant to superradiant eigenmodes can be understood by the appearance and disappearance of Bragg diffraction peaks of the scattered radiation. Because of this, it was shown that there exists a collection of eigenmodes that have no diffraction peaks at all when $a < \lambda/2$ and therefore *do not radiate*. Finally, it was shown that these divergences and discontinuities in the band structure of an array may be exploited in order to control the photon scattering rate by changing the angle of the driving laser, allowing one to manipulate the collective Lamb shift as well as access subradiant eigenmodes even when the size of the sample is much larger than λ.

It has been suggested that coherently radiating systems should be thought of in terms of Bragg scattering [12,27,43], where the radiators have certain spatially dependent phase correlations. Here, this picture is necessary. This is because the symmetries in an atomic array cause the number of diffraction peaks to change. Since photons are mainly emitted into these diffraction peaks [27], the photon scattering rate changes drastically with their appearance and disappearance. In systems such as cold atom gases, where the spatial distribution of atoms is highly disordered, the spatially dependent phases caused by the driving laser still cause a diffraction peak in the forward direction. This phenomenon is, of course, the well-known coherent forward scattering [20,25]. A large part of understanding the nature of radiators in the low excitation regime essentially consists of determining the spatially dependent phase relationship between atoms followed by determining their resulting scattered emission. Recently, interesting new physics has resulted from approximating this relationship as the one caused by the initial driving laser, i.e., the timed Dicke state [6,7,16,20]. Understanding the nature of how these phase relationships develop and how they may be manipulated in order to explore new physical systems will surely provide novel insights into the relationship between light and matter in the future.

Note added. The authors have recently become aware of work by Jen *et al.* [44] that studies the appearance of subradiant states in finite arrays of atoms. This contains some similar ideas to those of Sec. IV.

ACKNOWLEDGMENT

The authors would like to thank Prof. C.-L. Hung for enlightening conversations, as well as Jesús Pérez-Ríos for his valuable insights into graphic design. This material is based upon work supported by the National Science Foundation under Grant No. 1404419-PHY.

[1] R. H. Dicke, Phys. Rev. **93**, 99 (1954).
[2] A. Goban, C.-L. Hung, J. D. Hood, S.-P. Yu, J. A. Muniz, O. Painter, and H. J. Kimble, Phys. Rev. Lett. **115**, 063601 (2015).
[3] D. D. Yavuz, J. Opt. Soc. Am. B **31**, 2665 (2014).
[4] R. Monshouwer, M. Abrahamsson, F. van Mourik, and R. van Grondelle, J. Phys. Chem. B **101**, 7241 (1997).
[5] M. A. Palacios, F. L. de Weerd, J. A. Ihalainen, R. van Grondelle, and H. van Amerongen, J. Phys. Chem. B **106**, 5782 (2002).
[6] R. T. Sutherland and F. Robicheaux, Phys. Rev. A **93**, 023407 (2016).
[7] S. Bromley, B. Zhu, M. Bishof, X. Zhang, T. Bothwell, J. Schachenmayer, T. L. Nicholson, R. Kaiser, S. F. Yelin, M. D. Lukin, A. Rey, and J. Ye, Nat. Commun. **7**, 11039 (2016).
[8] R. A. de Oliveira, M. S. Mendes, W. S. Martins, P. L. Saldanha, J. W. R. Tabosa, and D. Felinto, Phys. Rev. A **90**, 023848 (2014).
[9] J. Javanainen, J. Ruostekoski, Y. Li, and S.-M. Yoo, Phys. Rev. Lett. **112**, 113603 (2014).
[10] T. Bienaimé, N. Piovella, and R. Kaiser, Phys. Rev. Lett. **108**, 123602 (2012).
[11] T. Ido, T. H. Loftus, M. M. Boyd, A. D. Ludlow, K. W. Holman, and J. Ye, Phys. Rev. Lett. **94**, 153001 (2005).
[12] M. O. Araújo, I. Kresic, R. Kaiser, and W. Guerin, arXiv:1603.07204.
[13] S. J. Roof, K. J. Kemp, M. D. Havey, and I. M. Sokolov, arXiv:1603.07268.
[14] J. Javanainen and J. Ruostekoski, Opt. Express **24**, 993 (2016).
[15] Z. Meir, O. Schwartz, E. Shahmoon, D. Oron, and R. Ozeri, Phys. Rev. Lett. **113**, 193002 (2014).
[16] M. O. Scully, Phys. Rev. Lett. **102**, 143601 (2009).
[17] R. Röhlsberger, K. Schlage, B. Sahoo, S. Couet, and R. Rüffer, Science **328**, 1248 (2010).
[18] J. Keaveney, A. Sargsyan, U. Krohn, I. G. Hughes, D. Sarkisyan, and C. S. Adams, Phys. Rev. Lett. **108**, 173601 (2012).
[19] M. Gross and S. Haroche, Phys. Rep. **93**, 301 (1982).
[20] M. Scully, Laser Phys. **17**, 635 (2007).
[21] W. Guerin, M. O. Araújo, and R. Kaiser, Phys. Rev. Lett. **116**, 083601 (2016).
[22] M. O. Scully, Phys. Rev. Lett. **115**, 243602 (2015).
[23] D.-W. Wang, R.-B. Liu, S.-Y. Zhu, and M. O. Scully, Phys. Rev. Lett. **114**, 043602 (2015).

[24] A. A. Svidzinsky, J.-T. Chang, and M. O. Scully, Phys. Rev. Lett. **100**, 160504 (2008).
[25] M.-T. Rouabah, M. Samoylova, R. Bachelard, P. W. Courteille, R. Kaiser, and N. Piovella, J. Opt. Soc. Am. A **31**, 1031 (2014).
[26] M. O. Scully, E. S. Fry, C. H. Raymond Ooi, and K. Wódkiewicz, Phys. Rev. Lett. **96**, 010501 (2006).
[27] D. Porras and J. I. Cirac, Phys. Rev. A **78**, 053816 (2008).
[28] C. Mewton and Z. Ficek, J. Phys. B: At., Mol. Opt. Phys. **40**, S181 (2007).
[29] J. P. Clemens, L. Horvath, B. C. Sanders, and H. J. Carmichael, Phys. Rev. A **68**, 023809 (2003).
[30] L. Ostermann, H. Zoubi, and H. Ritsch, Opt. Express **20**, 29634 (2012).
[31] H. Zoubi, Europhys. Lett. **100**, 24002 (2012).
[32] R. J. Bettles, S. A. Gardiner, and C. S. Adams, Phys. Rev. A **92**, 063822 (2015).
[33] R. J. Bettles, S. A. Gardiner, and C. S. Adams, Phys. Rev. Lett. **116**, 103602 (2016).
[34] A. A. Svidzinsky, J.-T. Chang, and M. O. Scully, Phys. Rev. A **81**, 053821 (2010).
[35] Z. Liao and M. S. Zubairy, Phys. Rev. A **90**, 053805 (2014).
[36] S. D. Jenkins and J. Ruostekoski, Phys. Rev. A **86**, 031602 (2012).
[37] J. Ruostekoski and J. Javanainen, Phys. Rev. A **55**, 513 (1997).
[38] J. D. Jackson, *Classical Electrodynamics*, Vol. 3 (Wiley, New York, 1999).
[39] D. C. Lay, *Linear Algebra and Its Applications*, 4th ed. (Addison-Wesley, Reading, MA, 2012).
[40] A. Burin, H. Cao, G. Schatz, and M. Ratner, J. Opt. Soc. Am. B **21**, 121 (2004).
[41] S.-T. Chui, S. Du, and G.-B. Jo, Phys. Rev. A **92**, 053826 (2015).
[42] R. Halir, P. J. Bock, P. Cheben, A. Ortega-Moñux, C. Alonso-Ramos, J. H. Schmid, J. Lapointe, D.-X. Xu, J. G. Wangüemert-Pérez, Í. Molina-Fernández *et al.*, Laser Photonics Rev. **9**, 25 (2015).
[43] A. Hilliard, F. Kaminski, R. Le Targat, C. Olausson, E. S. Polzik, and J. H. Müller, Phys. Rev. A **78**, 051403 (2008).
[44] H. H. Jen, M.-S. Chang, and Y.-C. Chen, Phys. Rev. A **94**, 013803 (2016).